Journal of Materials Chemistry B

RSC Publishing

PAPER

View Article Online
View Journal | View Issue

Cite this: *J. Mater. Chem. B*, 2013, **1**, 512

Graphene oxide based fluorescent nanocomposites for cellular imaging†

Yang Sheng, Xiaosheng Tang, Erwin Peng and Junmin Xue*

Received 16th September 2012
Accepted 6th November 2012

DOI: 10.1039/c2tb00123c

www.rsc.org/MaterialsB

Carbon based 2-D material graphene oxide (GO) is a promising platform for preparing composites for biomedical applications because of its superior water solubility and low toxicity. Herein, we reported a convenient route to prepare fluorescent nanocomposites incorporating water-soluble GO sheets and Zn doped $AgInS_2$ nanoparticles. According to the study, the photoluminescence of the Zn doped $AgInS_2$ nanoparticles was well maintained after the hybridization using GO. No obvious emission shift was observed and the PL intensity was stable for over three months with negligible quenching. The PEGylated AIZS–GO nanocomposites could be readily up-taken by NIH/3T3 cells (mouse embryonic fibroblast cell line) while no distinct cytotoxicity was observed. The subsequent *in vitro* cellular imaging of NIH/3T3 cells proved that the as-prepared AIZS–GO–PEG nanocomposites were potential fluorescent probes for biomedical targeting and imaging.

1 Introduction

Graphene and its derivatives have attracted a lot of attention due to their unique physical and chemical properties and promising future in various application areas.[1–6] Graphene oxide (GO), a derivative of graphene prepared from natural graphite, emerges as an attractive candidate for biomedical purposes because of its chemical inertness, biocompatibility and low toxicity.[7] Unlike hydrophobic graphene, GO can be readily dispersed in water because there are many hydrophilic oxygenated functional groups at its edges and basal planes such as epoxy, hydroxyl and carboxyl.[8,9] These functional groups not only promote the water solubility, but also favor the modification of GO with other molecules *via* covalent or non-covalent bondings.[10,11] Due to these extraordinary features, GO is extremely suitable for biomedical applications such as drug delivery and cellular imaging.[12–15]

Compared to the micron sized graphene material, which is preferred in developing electronic devices, sub-100 nm graphene oxide is more favorable and advantageous for biomedical applications. In this sense, graphene quantum dots for both bio-imaging and drug delivery have been reported by cutting the size down into the sub-10 nm range using ultrasonication or plasma treatment, followed by filtration.[16–18] However, so far it is still not easy to obtain strong luminescent graphene or graphene oxide with tunable emissions.[7,19,20] On the other hand, semiconductor nanoparticles have been systematically studied to control the composition and photoluminescence (PL).[21,22] However, well-controlled semiconductor nanoparticles are usually synthesized from thermal decomposition in non-polar solvents,[23] thus they lack good water solubility and their surface modifications are complicated. Therefore it could be advantageous if there is a convenient route to incorporate semiconductor nanoparticles into GO to make a composite with tunable PL emission and versatile surface functionality.[24,25]

Hitherto there have been a few publications reporting the synthesis of nanocomposites based on semiconductor quantum dots and GO, including GO–CdTe and GO–CdS by using *in situ* deposition or electrostatic assembly techniques.[26,27] Nevertheless the quantum dots (QDs) used in these reports are all based on cadmium, a well-known toxin and suspected carcinogen.[28] Although coating techniques have been developed to reduce the cytotoxicity of QDs by preventing direct contact with target tissues and cells, peoples' concern about the potential leaking of Cd ions remains. In this sense, ternary I–III–VI_2 chalcopyrite type semiconductor nanoparticles such as $AgInS_2$ and $CuInS_2$ become good alternative Cd-free cell labeling agents.[29] In the past several years, many efforts have been made on synthesizing I–III–VI_2 semiconductors with well controlled size, morphology and PL emission.[30]

Herein we report the successful synthesis of sub-100 nm fluorescent nanocomposites consisting of zinc-doped $AgInS_2$ (AIZS) nanoparticles and GO for cellular imaging applications. The procedure for the formation of the composites is illustrated in Scheme 1. Generally, the GO was prepared by using the modified Hammers' method. Water-soluble GO sheets were subsequently modified with oleylamine to render partial hydrophobicity in order to be dispersed in chloroform. Following that,

Department of Materials Science and Engineering (DMSE), National University of Singapore (NUS), 7 Engineering Drive 1, Singapore 117574. E-mail: msexuejm@nus.edu.sg

† Electronic supplementary information (ESI) available. See DOI: 10.1039/c2tb00123c

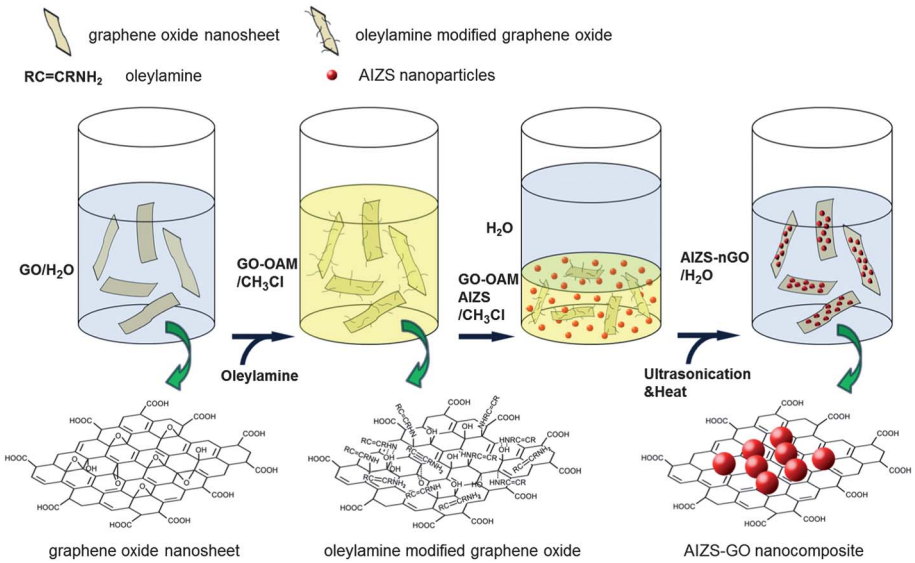

Scheme 1 Schematic illustration of the procedure for synthesizing fluorescent AIZS–GO nanocomposites.

the freshly prepared hydrophobic AIZS nanoparticles without any surface modification were assembled onto the oleylamine modified GO *via* a micro-emulsion technique. In this study, the emission colors of the AIZS decorated GO (AIZS–GO) could be easily tuned by changing the doping amount of Zn in AIZS nanoparticles and thus AIZS–GO nanocomposites with green, yellow, orange and red colors were prepared. Compared to other phase transfer methods such as ligand exchange and silica coating,[31] the method we used is more effective in preserving the PL property owing to the hydrophobic–hydrophobic interaction between the AIZS nanoparticles and GO, which does not deteriorate the surface of AIZS nanoparticles. The emission of the nanocomposites exhibited no obvious shift in wavelength, while the PL intensity has an insignificant decrease after the hybridization. Although it was found that the negatively charged groups from GO led to instability in phosphate buffered saline (PBS) solution, PEGylation of the nanocomposites using EDC/NHS chemistry could improve the colloidal stability in PBS solution. The PEGylated AIZS–GO nanocomposites demonstrated low cytotoxicity, successful cell up-take and imaging by utilizing the NIH/3T3 cell line as a model.

2 Experimental procedures

Synthesis of graphene oxide (GO) and subsequent surface modification

GO was synthesized using modified Hammers' method.[32] Typically, 0.5 g graphite (2–15 μm), 0.5 g $NaNO_3$, and 23 mL H_2SO_4 were mixed together in an ice bath, while $KMnO_4$ was added slowly into the mixture. The obtained green sticky mixture was left to stir for one hour before it was heated up to 35 °C overnight. Approximately 20 mL of H_2O was added drop wise at the beginning because the mixture was very thick. Besides, a lot of heat could be generated during the process and the mixture might go through a burst in temperature if water was added too fast. Following that, a volume of 100 mL of H_2O was added. After 12 hours, 3 mL H_2O_2 were added drop by drop into the brown solution. The final product was washed with 4% HCl and DI-H_2O repeatedly until the solution reached almost neutral. The obtained graphite oxide solution was ultrasonicated for 2 hours at 20 GHz (130 W), followed by centrifugation at 10 000 rpm for 30 minutes to remove the precipitate which contained large GO sheets.

To prepare oleylamine modified GO (OAM-GO) nanosheets, the GO solution (containing ~50 mg GO) was dried and then sonicated with 6 mL oleylamine and 10 mL hexane for 1 hour. Centrifugation was performed to remove the unreacted GO and other precipitates. A black suspension of OAM-GO was obtained.

Synthesis of zinc doped $AgInS_2$ (AIZS) nanoparticles

AIZS nanoparticles were synthesized according to the previous report with some modifications.[30] Typically, to synthesize AIZS nanoparticles with orange emission, 0.1 mM indium acetate, 0.1 mM silver nitrate, 0.1 mM oleic acid, 2 mM *n*-dodecanethiol (DDT), 50 μL trioctylphosphine (TOP), and 4 mL of 1-octadecene (ODE) were loaded into a three-neck flask. The mixture was then heated to 150 °C and 0.1 mM sulfur dissolved in ODE and oleylamine was injected at this point. 10 minutes later, 0.1 mM zinc stearate dissolved in ODE was injected (~150 μL). The mixture was then heated to 210 °C quickly, followed by adding 10 drops of zinc stearate/ODE solution and annealing at this temperature for 30 minutes. The mixture was then cooled down to room temperature. The product was collected by adding ethanol and centrifuging. The collected AIZS nanoparticles were then dispersed in hexane and washed with ethanol and acetone repeatedly for purification. The final product was dispersed in hexane or chloroform. As suggested by the reference, the emission colors of the AIZS nanoparticles were easily tuned by adjusting the injection temperature of S and Zn sources. In this

study, the AIZS nanoparticles with green, yellow, and red emission were prepared by using the injection temperatures of 70 °C, 120 °C and 180 °C, respectively.

Assembly of AIZS nanoparticles on OAM-GO (AIZS–GO) sheets

To synthesize AIZS–GO nanocomposites, the AIZS nanoparticles were dispersed in chloroform first. The OAM-GO sheets were washed to remove extra oleylamine by adding 2 times excess volume of ethanol. Approximately 1 mg of OAM-GO sheets were then suspended in 900 μL chloroform by sonication. Then 300 μL AIZS suspension was mixed with the OAM-GO solution. 10 times volume of DI-H_2O was then added into the mixture and ultrasonication was carried out to form a stable turbid suspension. The suspension was then heated to 60 °C for 30 minutes to evaporate the chloroform. During the heating process, the turbid solution gradually turned transparent, indicating the successful assembly of the AIZS nanoparticles on the GO sheets.

The fluorescence quantum yield (QY) was determined by comparing the integrated fluorescence intensity over the absorbance of sample's solutions with that of a standard organic fluorescent dye (fluorescein in H_2O, QY95%, Rhodamine B and Rhodamine 101 in ethanol, QY100%). The absorbance of all solutions was below 0.1 at the excitation wavelength (365 nm). Four different concentrations for each sample were tested for determining the QY.

PEGylation of AIZS decorated GO sheets (AIZS–GO–PEG)

Before the colloidal stability, cytotoxicity and cell imaging tests, the AIZS–GO nanocomposites were conjugated with PEG. Typically, 5 mL (~10 mg AIZS–GO) was mixed with 10 mL aqueous solution of PEG containing 150 mg methoxyl PEG amine (mPEG–NH_2, M_w 2000). 2.5 mL EDC aqueous solution (1 mg mL^{-1}) and 2.5 mL NHS aqueous solution (1 mg mL^{-1}) were added subsequently. This mixture was then left to stir for over 24 hours to complete the conjugation. The concentration of the prepared AIZS–GO–PEG was measured to be 136 μg mL^{-1} based on AIZS nanoparticles by elemental analysis (ICP). The final product was dialyzed to remove the unreacted PEG, EDC and NHS and byproducts using a dialysis membrane (molecular weight cut-off: 3 kDa). After the dialysis, a solution of concentration 100 μg mL^{-1} was obtained *via* dilution for further experiments. The AIZS–GO–PEG nanocomposites were dispersed in DI-H_2O and phosphate buffered saline (PBS 1×, pH 7.4) solutions for colloidal stability tests.

In vitro cytotoxicity of AIZS–GO–PEG on NIH/3T3 fibroblast cells

To assess the cytotoxic effect of the final product AIZS–GO–PEG nanocomposites, *in vitro* cell viability tests were performed by incubating NIH/3T3 cells with the nanocomposites at different concentrations for 24 hours using a CCK-8 assay. NIH/3T3 fibroblast cells were grown in DMEM (Dulbecco's Modified Eagle Medium) culture growth medium (10% bovine calf serum) at 37 °C in a 5% CO_2 humidified environment. The cells were then transferred to a 96-well cell culture plate (TPP 96) at an identical concentration of 7.5×10^4 cells per mL (0.1 mL). These cells were incubated overnight under the same conditions before the addition of the AIZS–GO–PEG nanocomposites. Following the incubation, 20 μL of the nanocomposites at different concentrations (from 100 μg mL^{-1} to 1 μg mL^{-1}) was added into each well. After that, the cells were incubated at 37 °C in a 5% CO_2 environment for 24 hours. Before the cell viability test, 10 μL cell counting kit-8 (CCK-8) was added into the culture media, followed by 4 hour incubation in the same environment. Absorbance readings were analyzed spectrophotometrically at 355 nm using a FluoStar Optima microplate reader.

In vitro cellular imaging of AIZS–GO–PEG on NIH/3T3 cells

To demonstrate the cellular imaging application of the AIZS–GO–PEG nanocomposites, NIH/3T3 fibroblast cells were chosen as a model. The cells were grown in DMEM culture growth medium at 37 °C in a 5% CO_2 humidified environment. The cells were then transferred to an 8-well cell culture plate at an identical concentration of 2.5×10^4 cells per mL (0.4 mL). The estimated number of cells in each well was approximately 1.0×10^4 cells. These cells were cultivated under the same conditions for 24 hours. Subsequently 10 μL of the AIZS–GO–PEG nanocomposites with different concentrations were added into desired wells, followed by another 24 hour incubation at 37 °C under 5% CO_2 conditions. Following the incubation, the cell cultures were rinsed 2 times to remove dead cells and extra nanocomposites. The cellular imaging was carried out using a confocal microscope (Leica TCS SP5X with MP). The samples were illuminated with a 50 mW diode laser at 405 nm.

Characterizations

The X-ray diffraction (XRD) patterns were obtained by an advanced diffractometer system (D8 Advanced Diffractometer System, Bruker, Karlsruhe, Germany). Transmission electron microscopy (TEM) images were obtained using a JEOL 3010 microscope at an acceleration voltage of 300 kV. Samples were prepared by dipping carbon-coated copper grids into the sample solution followed by drying in an ambient environment. UV-Vis absorption spectra were recorded using a Shimadzu UV-1601 UV-Vis spectrophotometer. The baselines were collected in the range of 350–800 nm with a sensitivity of 1 nm in hexane and de-ionized water, respectively. Photoluminescence (PL) spectra were collected in an open-sized 1 cm path-length quartz using a LS 55 Perkin-Elmer luminescence spectrometer. FT-IR spectra were recorded on a Varian 3100 FT-IR (Excalibur series) spectrophotometer. Samples were prepared by casting pellets from sample/KBr mixtures and 64 scans were signal averaged with a resolution of 4 cm^{-1} at room temperature.

3 Results and discussion

Fig. 1A shows the AFM image of the obtained GO. It was observed that the obtained GO flakes had a quite wide size range. Most of the flakes were less than 100 nm but with some exceptional big flakes which are larger than 100 nm. The inset

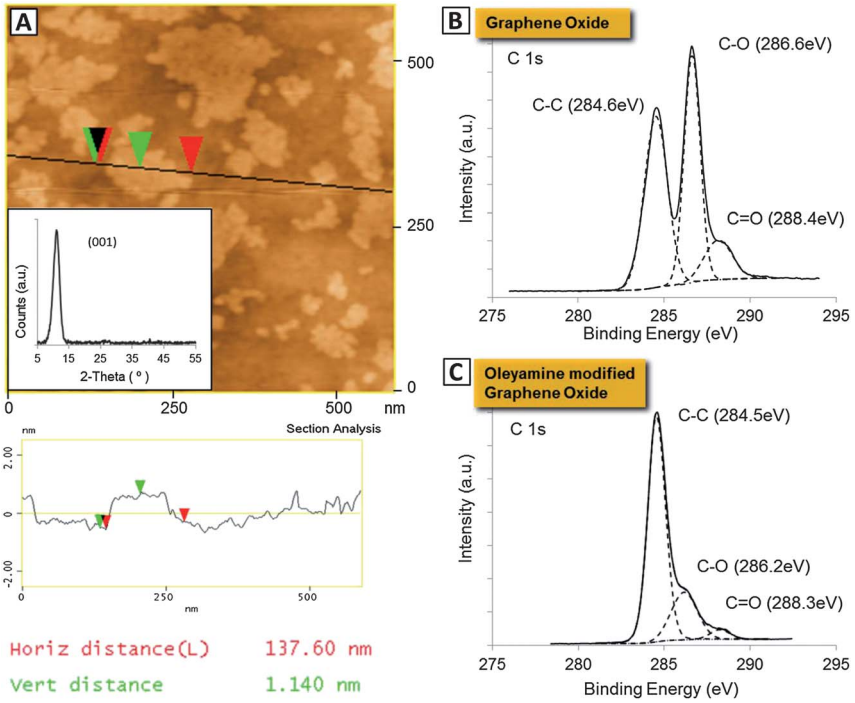

Fig. 1 (A) AFM image of the obtained GO (inset: XRD pattern of the corresponding GO). XPS spectra of GO (C 1s) (B) and oleyamine modified GO (C 1s) (C).

displays the XRD pattern of the corresponding GO. The sharp peak that appeared at 10.2° corresponded to the (001) reflection of graphene oxide.[33] It indicated that the spacing between sheets was 0.865 nm (ESI†), which was caused by the oxygenated groups in between the sheets. The obtained GO has also been characterized by X-ray photoelectron spectroscopy (XPS). The XPS spectrum (Fig. 1B) showed distinct peaks of C–O (286.6 eV) and C═O (288.4 eV) bonds apart from the C–C bond (284.6 eV), suggesting that the graphite had been successfully oxidized to graphene oxide (GO). The existence of –OH (~3400 cm^{-1}), C═O (~1700 cm^{-1}) and C═C (~1600 cm^{-1}) functional groups on GO were also observed in the FT-IR spectra (ESI, Fig. S1(i)†). After the modification with oleylamine, the XPS spectrum was also analyzed. Fig. 1C shows that the C–O bond of the oleylamine modified GO (OAM-GO) was significantly decreased. Therefore the obtained C–C/C–O ratio increased dramatically from about 0.8 (Fig. 1B) to 4.2 (Fig. 1C), indicating that the majority of C–O–C bonds have successfully reacted with oleylamine. The FT-IR spectrum (ESI, Fig. S1(ii)†) of OAM-GO also revealed two peaks at ~2850 cm^{-1} and ~2950 cm^{-1} which belonged to C–H stretch from oleylamine. The modification by OAM could be attributed to the following mechanisms. The first one was the ring opening of the triangular epoxy group (C–O–C) induced by alkylamine. Under extended ultrasonication, the basal epoxy group on GO reacted with amine through nucleophilic attack, leading to the covalent bonding between the C from epoxy and N from amine (C–N bond, refer to the ESI, Fig. S2†).[34] In addition, the non-covalent binding might also occur between oleylamine and GO. As indicated by the C–C bond and C═C bond from the XPS and FT-IR data, some parts on GO were not oxidized. Thus there was a possibility that the non-polar tail of oleylamine could be attracted to these hydrophobic parts on the basal plane of GO *via* van der Waals interactions.[3] Meanwhile, oleylamine could also non-covalently interact with GO *via* hydrogen bonding between respective amine and hydroxyl groups.[3]

The AIZS nanoparticles with four different emission colors were prepared *via* a thermal decomposition route. The TEM images (Fig. 2A–D) show AIZS nanoparticles with green, yellow, orange and red emissions synthesized at four different injection temperatures, respectively. The average diameter of the nanoparticles with green and yellow emissions was about 3–4 nm, while that of the nanoparticles with orange and red emissions was approximately 6–7 nm. The emission colors were conveniently tuned by adjusting the injection temperatures of sulfur and zinc stearate precursors. The detailed synthesis procedure is available in our recent publication.[30] As shown in the XRD patterns (Fig. 2E), the diffraction peaks of the obtained AIZS nanoparticles were shifted from $AgInS_2$ towards ZnS when the emission color shifted from red to green. The observed peak shift indicated that more zinc ions were diffused into the matrix of the $AgInS_2$ when the injection temperature decreased.[30] The as-prepared AIZS nanoparticles were covered with hydrophobic ligands such as oleylamine, 1-dodecanethiol and TOPO, which could be proven by FT-IR spectra (ESI, Fig. S1(iii)†). The TGA diagram (ESI, Fig. S3†) showed that the surfactants on the surface took approximately 47 wt% of the total weight of the obtained AIZS nanoparticles. After being washed thoroughly, the AIZS nanoparticles were stored in chloroform and ready to be decorated on OAM-GO sheets.

The AIZS–GO nanocomposites were prepared by applying ultrasonication and heat-up processes. The GO was pre-modified with oleylamine. Therefore the OAM-GO rendered partial

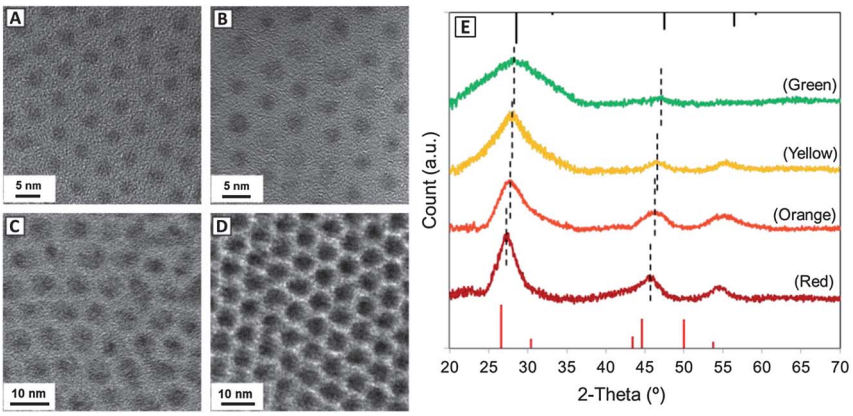

Fig. 2 TEM images of AIZS nanoparticles with green (A), yellow (B), orange (C) and red (D) emissions. (E) XRD patterns of AIZS nanoparticles with green, yellow, orange and red emissions, respectively.

hydrophobicity which allowed it to be suspended in chloroform. In the meantime, the AIZS nanoparticles were also hydrophobic as they were covered by non-polar surfactants such as oleylamine, oleic acid and dodecanethiol. During ultrasonication, small droplets containing chloroform, AIZS nanoparticles and OAM-GO were formed and stabilized. When chloroform was evaporated as the mixture was heated up, the AIZS nanoparticles were gradually pushed towards OAM-GO by the water–chloroform interface and eventually encapsulated by the hydrophobic chains of OAM-GO. The AIZS nanoparticles interacted with OAM-GO *via* van der Waals forces between respective hydrophobic parts. The AFM and TEM images of the corresponding AIZS–GO nanoparticles with red emission are displayed in Fig. 3. The TEM image (Fig. 3A) shows that the obtained AIZS–GO nanocomposites were dispersed well in water, as no aggregation was observed. It could also be seen that these AIZS–GO nanoparticles were no larger than 100 nm. The DLS measurement (Fig. 3B, inset: bottom right) exhibited a consistent result, revealing a *Z*-average size of ~75 nm. One typical AIZS–GO nanocomposite is also shown in the inset of Fig. 3A. The single layer of AIZS nanoparticle assembly could be clearly observed in the image, while the GO was difficult to be seen due to its low contrast. Therefore, AFM analysis upon the AIZS–GO nanocomposites was utilized to further verify their dimensions. The AFM image (Fig. 3B) shows consistency with the TEM image. Well dispersed AIZS–GO nanoparticles could be clearly seen on the silicon substrate. The high resolution AFM image (Fig. 3C) of one typical AIZS–GO nanoparticle revealed that its size was approximately 70 nm in diameter and ~7 nm in height. These results were consistent with the above DLS measurement and TEM observation where the AIZS–GO nanoparticles were smaller than 100 nm and the assembly of AIZS nanoparticles on the GO sheets was single-layered.

The insets in Fig. 3B clearly show that the red emitting AIZS nanoparticles were successfully transferred from non-polar organic solution to aqueous solution by OAM-GO. Compared to the solution of original red emitting AIZS nanoparticles, the AIZS–GO aqueous solution appeared to be darker under room light conditions. This was because of the existence of blackish GO in the solution. The left photograph displays the samples under UV irradiation. No distinct emission color change was observed, which could be further verified in PL characterization (will be discussed in the following section). Meanwhile the excitation spectra (ESI, Fig. S4†) showed no distinct difference between the original AIZS nanoparticles dispersed in hexane and the AIZS–GO nanocomposites suspended in H_2O. In addition, the XRD pattern of the nanocomposites with red emission showed no obvious shift in the identical peaks of AIZS

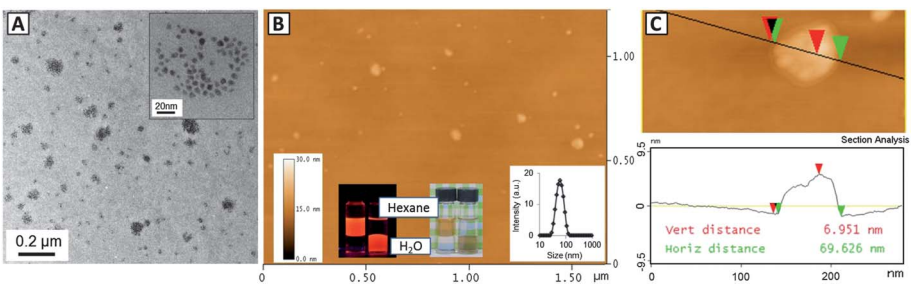

Fig. 3 (A) TEM image of the as-synthesized AIZS–GO nanocomposites with red emission (inset: TEM image of one AIZS–GO nanocomposite). The GO sheets are not observable in the images due to low contrast. (B) AFM image of the corresponding AIZS–GO nanocomposites (insets from left to right: photographs of red emitting AIZS nanoparticles and AIZS–GO nanocomposites under room light (right) and UV lamp irradiation (left) conditions; DLS measurement of the corresponding AIZS–GO nanocomposites). (C) High-resolution AFM image of the AIZS–GO nanocomposites.

nanoparticles after the hybridization (data not shown). The above information suggests that the AIZS nanoparticles were protected well during the synthesis process.

Thereafter, the same synthesis procedure was applied to orange, yellow and green emitting AIZS nanoparticles. The AIZS nanoparticles with orange emission possessed a similar average size to the red AIZS nanoparticles in this study, thus the corresponding AIZS–GO nanocomposites exhibited a similar morphology in TEM images (Fig. 4A and D). Both the DLS measurements (Fig. 4A, inset) and the TEM image indicated that the average size of the nanocomposites with orange emission was below 100 nm. However the AIZS nanoparticles with green or yellow emissions were very small in size, their contrasts were hence very low in TEM images (Fig. 4B and C, respectively). The assembly of these AIZS nanoparticles on OAM-GO could only be clearly observed in TEM images at high magnification (Fig. 4E and F, respectively). Although it turned out to be difficult to estimate the dimensions of the green and yellow emitting AIZS–GO nanocomposites by TEM observation, the DLS measurements suggested that their hydrodynamic sizes were about 66 nm and 70 nm, respectively.

Apart from the morphology, it was very important to maintain the photophysical properties after the QDs were transferred to an aqueous environment. The photoluminescence of AIZS nanoparticles and AIZS–GO nanocomposites with different emission colors were characterized and are compared in Fig. 5. Besides, the basic characteristics such as the mass ratio, hydrodynamic size, and quantum yields (QYs) are summarised in Table 1. Unlike some other phase transfer methods such as ligand exchange and silica coating,[31] which reduce and shift the emission of QDs significantly, the route we adopted here maintained the emissions of the QDs well. As shown in Fig. 5 and Table 1, the emission peak had a negligible shift after the AIZS nanoparticles were assembled on the GO sheets. On the other hand, the QY of the AIZS–GO nanocomposites had a relatively insignificant decrease compared to the original hydrophobic AIZS nanoparticles (Table 1). It was believed that the surface and structure of the AIZS nanoparticles were not deteriorated during the assembly. As specified in the experiments, the entire fabricating procedure of the nanocomposites only involved short time sonication and heating at 60 °C. Thus the surface ligands were not likely to be significantly detached from the AIZS nanoparticles under such circumstances. The FT-IR spectra of OAM-GO and ligands protected AIZS nanoparticles shared the same critical peak position at ~2900 cm^{-1} which was the characteristic peak for molecules containing a lot of C–H bonds. It could be an indicator to verify the surface ligands. As shown in Fig. S1(ii),† the transmittance peaks at ~1600 cm^{-1} and ~3400 cm^{-1} were from C=C and O–H bonds of the OAM-GO, respectively. It could be seen that after the incorporation of AIZS nanoparticles, the peaks at ~1600 cm^{-1} and ~3400 cm^{-1} decreased evidently while the peak at ~2900 cm^{-1} exhibited no obvious change (Fig. S1(iv)†), compared to the original OAM-GO (Fig. S1(ii)†). This change in ratio could only be attributed to the ligand signal from AIZS nanoparticles, indicating that the nanoparticles, which had abundant surface ligands, had been successfully deposited on the GO flakes. This verified that the surface ligands on AIZS nanoparticles were maintained, otherwise there would be no such distinct peak ratio change. Indeed, the AIZS nanoparticles were assembled onto the GO nanosheets by the hydrophobic–hydrophobic interaction between the alkane chains from both components.[35] However, the decrease in the QY was observed, which could be ascribed to the following reasons. First of all, although the synthesis of

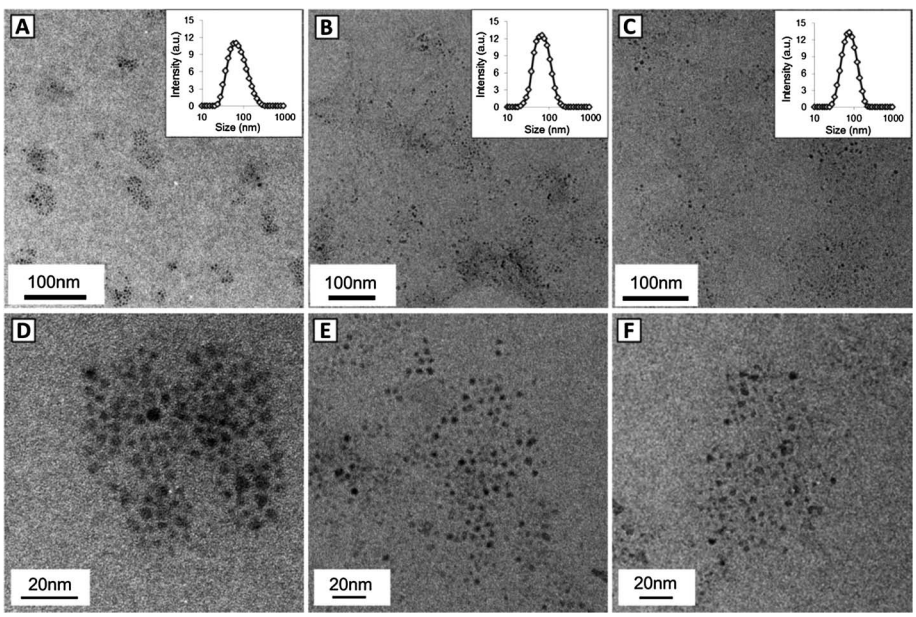

Fig. 4 TEM images of AIZS–GO nanocomposites with (A) orange, (B) yellow, and (C) green emissions in DI-H_2O. (D–F) TEM images of one AIZS–GO nanocomposite with orange, yellow, and green emissions, respectively. Insets in (A)–(C) are their corresponding DLS measurements. The GO sheets are not observable in the images due to low contrast.

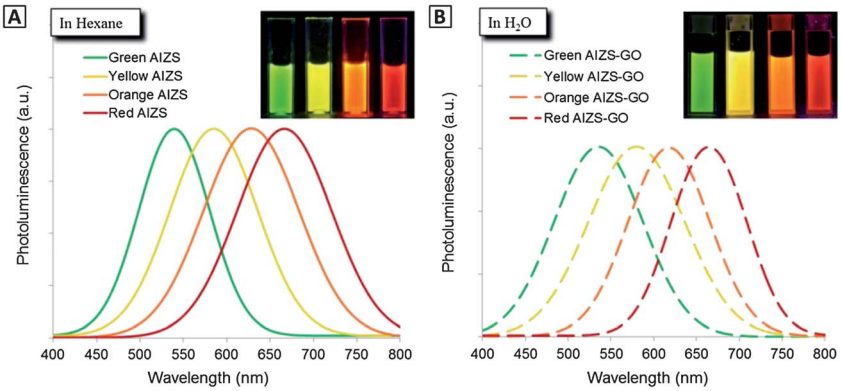

Fig. 5 (A) The photoluminescence spectra of AIZS nanoparticles suspended in hexane (inset: photograph of the corresponding AIZS nanoparticles under UV lamp irradiation). (B) The photoluminescence spectra of AIZS–GO nanocomposites suspended in DI-H_2O (inset: photograph of the corresponding AIZS–GO nanocomposites under UV lamp irradiation).

Table 1 Summary of basic characteristics of the AIZS–GO nanocomposites

Sample name	*Z*-average[a] (nm)	*Z*-average[b] (nm)	Emission[c] (nm)	Emission[d] (nm)	QY[e] (a.u.)	QY (a.u.)[f]
Red AIZS–GO	79	63.5	667	664	31.7%	18%
Orange AIZS–GO	80.1	66.2	626	618	35.9%	20%
Yellow AIZS–GO	99.4	65.5	585	580	46.7%	27%
Green AIZS–GO	99	69.5	536	534	33.5%	18%

[a] *Z*-average obtained using 10 min ultrasonication. [b] *Z*-average obtained using 20 min ultrasonication. [c] Original AIZS nanoparticles dispersed in hexane. [d] AIZS–GO nanocomposites dispersed in DI-H_2O. [e] QY of original AIZS nanoparticles dispersed in hexane. [f] QY of AIZS–GO nanocomposites dispersed in DI-H_2O.

AIZS–GO nanocomposites did not include any ligand exchange process, it was still possible that a small fraction of these surface ligands was dissolved in the large quantity of aqueous solution. More importantly, unlike the non-polar solvent where the existence of species such as oxygen and hydroxide ions was negligible, there were large quantities of such ions in aqueous solution. Therefore it was possible that the AIZS nanoparticles were slightly corroded by the ions during the ultrasonication and chloroform evaporation processes, which in turn affected the PL intensity.[36] Additionally, the blackish GO absorbed visible light, therefore the emission from AIZS nanoparticles could be diminished in the presence of GO.

Although the as-prepared AIZS–GO nanocomposites showed good stability in DI-H_2O as there was no aggregation observed under room conditions for over three months, they were not stable in phosphate buffered saline (PBS 1×, pH 7.4) solution. Aggregation occurred within 30 minutes upon adding AIZS–GO nanocomposites into the PBS solution. This was probably because of the negatively charged oxygenated groups such as –OH and –COOH of GO. The electrostatic repulsion between the nanocomposites was easily disturbed and screened by the ions in PBS solution. Therefore polyethylene glycol (PEG) was grafted to the nanocomposites in order to improve the stability of the nanocomposites in ionic solutions. The introduction of PEG not only stabilized the nanocomposites by steric repulsion, but also prevented nanocomposites from protein absorption in the physiological environment, which could further favor the subsequent cytotoxicity test and application.

The AIZS–GO nanocomposites with red emission were chosen as a model for the PEGylation. It was noticed that there were carboxylic acid groups at the edges of GO, which could be utilized to form peptide bonds with amino group terminated PEG. Therefore the conjugation was carried out by applying EDC/NHS chemistry. FT-IR characterization (ESI, Fig. S1(iv and v)†) confirmed the successful conjugation of mPEG–NH_2 by comparing the transmittances (~800 cm^{-1} to ~1500 cm^{-1}) from samples AIZS–GO and AIZS–GO–PEG. After the conjugation, the colloidal stability of the nanocomposites was recorded using DLS. The measurements were performed in both DI-H_2O and PBS 1× solution. As shown in Fig. 6A, the *Z*-average size of the sample AIZS–GO–PEG in DI-H_2O was increased to approximately 95 nm, which was slightly bigger than that before the PEGylation. The subsequent DLS results showed that the *Z*-average size of the nanocomposites had no further change in DI-H_2O at both 25 °C and 37 °C over 36 hours. The corresponding TEM image (Fig. 6B) also verified that the

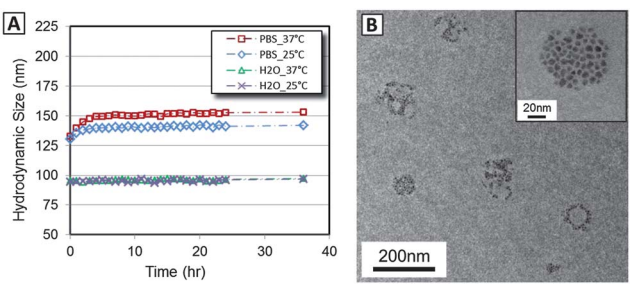

Fig. 6 (A) Colloidal stability of AIZS–GO–PEG nanocomposites measured at 25 °C and 37 °C in DI-H_2O and PBS solution, respectively. (B) TEM image of AIZS–GO–PEG nanocomposites dispersed in DI-H_2O (inset: one typical AIZS–GO–PEG nanocomposite).

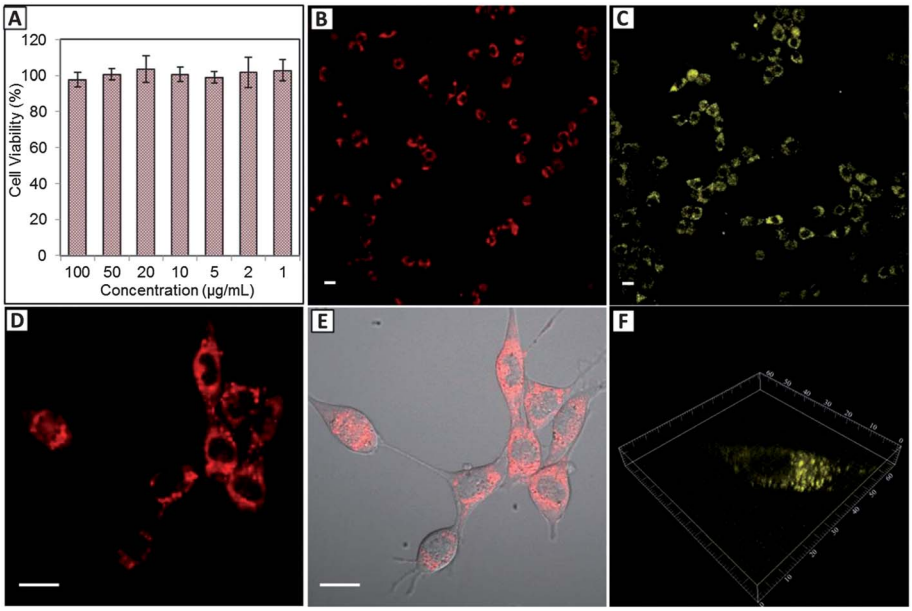

Fig. 7 (A) Dose-dependent viability evaluation of NIH/3T3 cells treated with AIZS–GO–PEG nanocomposites. Fluorescent images of NIH/3T3 cells tagged with red (B) and yellow (C) emitting AIZS–GO–PEG nanocomposites. (D and E) Fluorescent image and merged image of NIH/3T3 cells at high resolution (scale bars: 20 μm). (F) 3D image of one cell tagged with yellow emitting AIZS–GO–PEG nanocomposites.

AIZS–GO–PEG nanocomposites had no aggregation or change in AIZS loading. One typical AIZS–GO–PEG nanocomposite approximately 80 nm in diameter is also shown in the inset. Hence it was implied that the size increment was not due to the aggregation but the PEG conjugation. The stability of the AIZS–GO–PEG nanocomposites in PBS 1× solution was also tested using DLS. Upon being dispersed in PBS solution, the hydrodynamic size of the nanocomposites was increased to around 130 nm. This was probably because of the slight aggregation induced by the interaction between the remnants of oxygenated groups and the ions in the PBS solution. At 25 °C, the *Z*-average size reached approximately 140 nm quickly and thereafter the size was stabilized. At 37 °C, the stable *Z*-average size was around 150 nm, which was 10 nm larger than that at 25 °C.

The PEGylated nanocomposites were then subjected to the cytotoxicity test and cellular imaging demonstration. In this study, the nanocomposites were based on Cd and Pd free semiconductors and non-toxic graphene oxide. The cell viability, however, was still necessary to be examined with caution. The *in vitro* cell viability test of the nanocomposites was

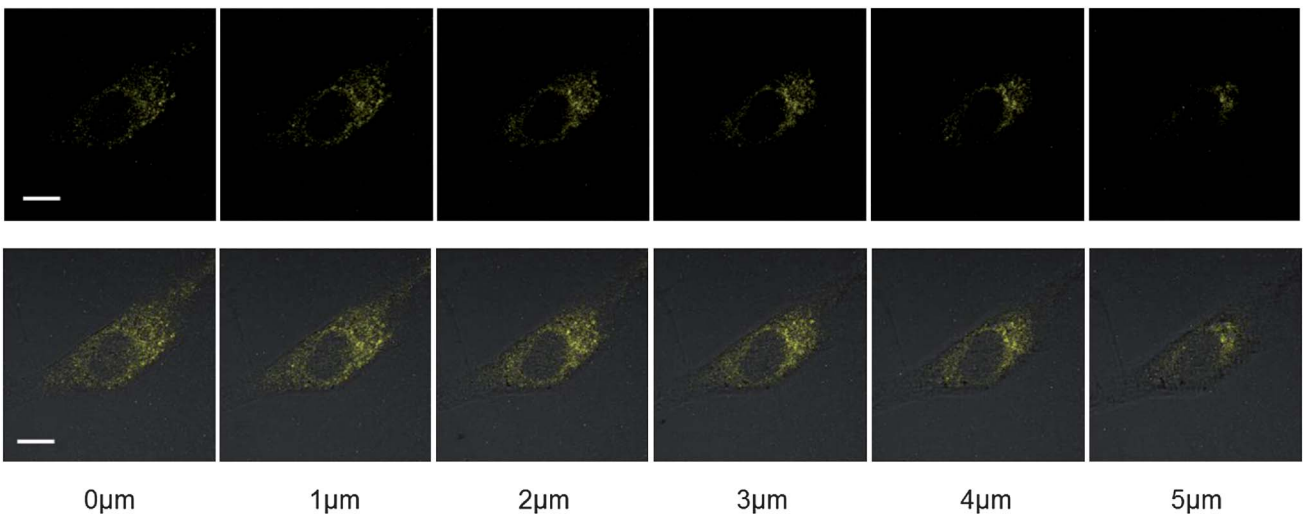

Fig. 8 CLSM images (top row) and merged images (bottom row) of one typical NIH/3T3 cell tagged with yellow color emitting AIZS–GO–PEG nanocomposites at different cross-sections (1 μm interval), illustrating the distribution of fluorescent nanocomposites in cell. Images were taken from the bottom to the top of the cell at a step of 0.5 μm. It could be clearly seen that the fluorescent nanocomposites were accumulated in cytoplasm around the nuclei (scale bars: 10 μm).

performed using NIH/3T3 cells. The nanocomposites of different concentrations were incubated with the cells at 37 °C for 24 hours before CCK-8 assay (based on the activity of the dehydrogenases of the living cells) was performed. The highest concentration of the nanocomposites used here was 100 μg mL^{-1} and the lowest was 1 μg mL^{-1}. As illustrated in Fig. 7A, no obvious cytotoxicity upon NIH/3T3 cells was observed as the concentration of the nanocomposites was increased from 1 μg mL^{-1} to 100 μg mL^{-1}. It is worth noticing that 100 μg mL^{-1} was in the concentration range for practical cellular staining with QD bioconjugates diluted in blood circulation under *in vivo* conditions.[37,38] This cytotoxicity result indicated that the obtained AIZS–GO–PEG nanocomposites had no significant cytotoxic effects upon the live cells.

The *in vitro* cellular imaging was also performed on the NIH/3T3 cell lines. The AIZS–GO–PEG nanocomposites with red and yellow emissions were chosen as the labeling agents to demonstrate the cellular imaging. The feasibility of using these nanocomposites to stain cells was demonstrated using a confocal laser scanning microscope (CLSM) with a laser source at 405 nm. Fig. 7B–F show the CLSM images of the NIH/3T3 cells after incubation with the AIZS–GO–PEG nanocomposites for 24 hours at an identical concentration of 50 μg mL^{-1}. It could be observed in high-resolution images (Fig. 7D and E) and in the 3D image (Fig. 7F) that the majority of the nanocomposites were accumulated in cytoplasm around the nuclei, which verified that the as-prepared AIZS–GO–PEG nanocomposites were successful cell labeling agents. More CLSM images are shown in the ESI, Fig. S5.† By comparing the bright field image and dark field image, it could be clearly seen that the AIZS–GO–PEG nanocomposites were successfully uptaken by the NIH/3T3 cells. Especially, *Z*-stack (0.5 μm step) has been performed on one particular cell labeled with yellow light emitting AIZS–GO–PEG nanocomposites. Fig. 8 displays the selected *z* stack images of the cell at a 1 μm interval. These images clearly show the distribution of the fluorescent nanocomposites in this particular cell at different cross-sections from its bottom to the top, indicating successful cell uptake and imaging.

4 Conclusions

In summary, we successfully synthesized fluorescent nanocomposites based on graphene oxide and AIZS nanoparticles. The AIZS–GO nanocomposites with four different emitting colors such as green, yellow, orange and red have been prepared and characterized. The average sizes of the obtained nanocomposites were below 100 nm, which favored various potential bio-applications especially *in vivo* bio-applications. The AIZS–GO nanocomposites showed bright emissions under UV irradiation as well as good water solubility. After the PEGylation, the colloidal stability of nanocomposites in PBS solution was prominently improved. The demonstration of cellular imaging using these nanocomposites was successful. Hereby, the sub-100 nm fluorescent nanocomposites combining AIZS and GO were proved to be promising candidates for future biomedical cellular imaging applications.

Acknowledgements

The authors are grateful for the financial support provided by Singapore MOE's AFR Tier 1 funding WBS R-284-000-088-112. The authors also thank Mr Neo Chin Yong and Ms Choo Swee Jen for their help in taking AFM images.

References

1 X. Huang, Z. Y. Yin, S. X. Wu, X. Y. Qi, Q. Y. He, Q. C. Zhang, Q. Y. Yan, F. Boey and H. Zhang, *Small*, 2011, **7**, 1876.
2 S. J. Guo and S. J. Dong, *Chem. Soc. Rev.*, 2011, **40**, 2644.
3 D. R. Dreyer, S. J. Park, C. W. Bielawski and R. S. Ruoff, *Chem. Soc. Rev.*, 2010, **39**, 228.
4 K. Zhang, L. L. Zhang, X. S. Zhao and J. H. Wu, *Chem. Mater.*, 2010, **22**, 1392.
5 S. J. Zhuo, M. W. Shao and S. T. Lee, *ACS Nano*, 2012, **6**, 1059.
6 T. N. Narayanan, B. K. Gupta, S. A. Vithayathil, R. R. Aburto, S. A. Mani, J. Taha-Tijerina, B. Xie, B. A. Kaipparettu, S. V. Torti and P. M. Ajayan, *Adv. Mater.*, 2012, **24**, 2992.
7 J. H. Shen, Y. H. Zhu, X. L. Yang and C. Z. Li, *Chem. Commun.*, 2012, **48**, 3686.
8 J. I. Paredes, S. Villar-Rodil, A. Martínez-Alonso and J. M. D. Tascón, *Langmuir*, 2008, **24**, 10560.
9 H. Q. Bao, Y. Z. Pan, Y. Ping, N. G. Sahoo, T. F. Wu, L. Li, J. Li and L. H. Gan, *Small*, 2011, **7**, 1569.
10 L. M. Zhang, J. G. Xia, Q. H. Zhao, L. W. Liu and Z. J. Zhang, *Small*, 2010, **6**, 537.
11 H. Bai, Y. X. Xu, L. Zhao, C. Li and G. Q. Shi, *Chem. Commun.*, 2009, 1667.
12 X. Y. Yang, X. Y. Zhang, Z. F. Liu, Y. F. Ma, Y. Huang and Y. S. Chen, *J. Phys. Chem. C*, 2008, **112**, 17554.
13 Z. Liu, J. T. Robinson, X. M. Sun and H. J. Dai, *J. Am. Chem. Soc.*, 2008, **130**, 10876.
14 X. M. Sun, Z. Liu, K. Welsher, J. T. Robinson, A. Goodwin, S. Zaric and H. J. Dai, *Nano Res.*, 2008, **1**, 203.
15 C. L. Zhang, Y. X. Yuan, S. M. Zhang, Y. H. Wang and Z. H. Liu, *Angew. Chem., Int. Ed.*, 2011, **50**, 6851.
16 X. L. Li, X. R. Wang, L. Zhang, S. W. Lee and H. J. Dai, *Science*, 2008, **319**, 1229.
17 Y. Li, Y. Hu, Y. Zhao, G. Q. Shi, L. E. Deng, Y. B. Hou and L. T. Qu, *Adv. Mater.*, 2011, **23**, 776.
18 Y. Li, Y. Zhao, H. H. Cheng, Y. Hu, G. Q. Shi, L. M. Dai and L. T. Qu, *J. Am. Chem. Soc.*, 2012, **134**, 15.
19 B. K. Gupta, P. Thanikaivelan, T. N. Narayanan, L. Song, W. Gao, T. Hayashi, A. L. M. Reddy, A. Saha, V. Shanker, M. Endo, A. A. Martí and P. M. Ajayan, *Nano Lett.*, 2011, **11**, 5227.
20 S. J. Zhu, J. H. Zhang, C. Y. Qiao, S. J. Tang, Y. F. Li, W. J. Yuan, B. Li, L. Tian, F. Liu, R. Hu, H. N. Gao, H. T. Wei, H. Zhang, H. C. Sun and B. Yang, *Chem. Commun.*, 2011, **47**, 6858.
21 M. Bruchez, M. Moronne Jr, P. Gin, S. Weiss and A. P. Alivisatos, *Science*, 1998, **281**, 2013.
22 R. G. Xie, M. Rutherford and X. G. Peng, *J. Am. Chem. Soc.*, 2009, **131**, 5691.

23 R. C. Han, M. Yu, Q. Zheng, L. J. Wang, Y. K. Hong and Y. L. Sha, *Langmuir*, 2009, **25**, 12250.
24 K. M. L. Taylor-Pashow, J. D. Rocca, R. C. Huxford and W. B. Lin, *Chem. Commun.*, 2010, **46**, 5832.
25 Y. H. Lee, L. Polavarapu, N. Y. Gao, P. Y. Yuan and Q. H. Xu, *Langmuir*, 2012, **28**, 321.
26 X. M. Zhao, S. W. Zhou, L. P. Jiang, W. H. Hou, Q. M. Shen and J. J. Zhu, *Chem.–Eur. J.*, 2012, **18**, 4974.
27 M. L. Chen, J. W. Liu, B. Hu, M. L. Chen and J. H. Wang, *Analyst*, 2011, **136**, 4277.
28 Y. Guo, D. L. Shi, H. S. Cho, Z. Y. Dong, A. Kulkarni, G. M. Pauletti, W. Wang, J. Lian, W. Liu, L. Ren, Q. Q. Zhang, G. K. Liu, C. Huth, L. M. Wang and R. C. Ewing, *Adv. Funct. Mater.*, 2008, **18**, 2489–2497.
29 D. S. Wang, W. Zheng, C. H. Hao, Q. Peng and Y. D. Li, *Chem. Commun.*, 2008, 2556.
30 X. S. Tang, W. X. B. A. Ho and J. M. Xue, *J. Phys. Chem. C*, 2012, **116**, 9769.
31 J. K. Oh, *J. Mater. Chem.*, 2010, **20**, 8433.
32 W. S. Hummers and R. E. Offeman, *J. Am. Chem. Soc.*, 1958, **80**, 1339.
33 T. Nakajima, A. Mabuchi and R. Hagiwara, *Carbon*, 1988, **26**, 357.
34 S. J. Park, D. A. Dikin, S. T. Nguyen and R. S. Ruoff, *J. Phys. Chem. C*, 2009, **113**, 15801.
35 E. S. G. Choo, X. S. Tang, Y. Sheng, B. Shuter and J. M. Xue, *J. Mater. Chem.*, 2011, **21**, 2310.
36 W. G. J. H. M. van Sark, P. L. T. M. Frederix, D. J. van den Heuvel, H. C. Gerritsen, A. A. Bol, J. N. J. van Lingen, C. de Mello Donegá and A. Meijerink, *J. Phys. Chem. B*, 2001, **105**, 8281.
37 X. G. Hu and X. H. Gao, *ACS Nano*, 2010, **4**, 6080.
38 X. Michalet, F. F. Pinaud, L. A. Bentolila, J. M. Tsay, S. Doose, J. J. Li, G. Sundaresan, A. M. Wu, S. S. Gambhir and S. Weiss, *Science*, 2005, **307**, 538.